# Characterization of a Small Helicopter UAV's Main Rotor Blade through Image Processing

*William J. Shipman, Yuko Roodt, Francois du Plessis*

Unmanned Aerial Vehicles Research Group
Department of Electrical and Electronic Engineering Science
University of Johannesburg, South Africa

`shipman.william@gmail.com`

## Abstract

Image processing is applied to the task of characterizing the response of a miniature helicopter's main rotor to collective control inputs under static conditions. The objective is to measure the pitch of the main rotor blade in relation to collective control inputs and deduce a transfer function model from the data. The algorithm developed here makes use of thresholding to perform image segmentation. Image moments are used to locate stickers placed on the edge of the rotor blade as markers. A high-speed camera was used to capture the motion of the rotor blade in digital video. This paper introduces the algorithm applied and explains the experimental setup.

## 1. Introduction

A miniature helicopter is controlled through its main and tail rotors by setting the pitch angles of these rotor blades. These control surfaces are, in turn, controlled by hobby servo motors, which in turn correspond to the standard controls found on all helicopters. These are the collective, the cyclic and the pedal controls. The speed with which these servo motors respond to control inputs determines the response of the control surfaces and hence, how quickly the control signal is able to affect the helicopter's flight. This transfer of the control signal from the servo motors' inputs to the helicopter's control surfaces is modelled by means of a transfer function. Knowledge of this model is required for control system design and testing. This paper will focus on the collective control to main rotor blade pitch angle transfer function only.

Traditionally, the characterization of the servo motors connected to the main rotor blade was done by means of some form of sensor attached to the main rotor blade to measure its pitch. For example, a potentiometer and analogue to digital converter can be used [1]. This type of experiment is normally performed under static conditions [2]. The load that the servo motors would experience in flight may be simulated by attaching a load [1], but work has been done where the main rotor blades were not loaded [2]. Alternatively, the potentiometer may be attached directly to the servo motor arm [3]. The linkages from the servo arm to the main rotor blades must be modelled to determine the resulting rotor blade pitch angle.

However, these methods [1] [2] have the disadvantage that physical contact with the rotor blade is required, or that the complex geometry of the mechanical linkages and swash plate must be determined [3]. An alternative approach followed at the University of Johannesburg makes use of a high-speed camera to record the motion of the rotor blade during ground experiments. In contrast to [3], the mechanical linkages are not modelled separately. This is beneficial as non-ideal properties such as friction in the mechanical linkages can be accounted for easily.

The experimental work was done under static conditions without any form of loading on the rotor blades. An image processing algorithm was developed to determine the orientation of the rotor blades from the recorded footage. This paper focusses on the image processing algorithm and the application of System Identification techniques to the characterization of main rotor blade pitch as a function of the collective control input.

The only motion considered in these experiments is the change in pitch angle as a function of the collective control input. Other motions, such as flapping, feathering or rotational motion caused by the helicopter's motor are not considered here or in the literature [1] [2] [3].

The lack of physical contact with the rotor blade is beneficial as it allows the experiment to be extended in the future to consider dynamic conditions where the helicopter's engine is turning the rotor blades. In comparison, techniques that require physical contact [1] [2] will be difficult to use under such conditions, as the measurement apparatus will have to move with the rotor blade.

Previously, $1^{st}$, $2^{nd}$ and $3^{rd}$ order transfer functions have been used to model the response of the main rotor blade pitch angle to servo command signals [3] [2] [1]. In all cases, frequency content is observed at up to $17\,\mathrm{Hz}$ when subjecting the servos to small-amplitude frequency sweeps. The frequency domain response and bandwidth of the rotor blades and servo motors is important for the design and verification of any future autopilots as this will limit their capabilities.

The experimental procedure required that a sinusoidal control input be supplied to the collective control. It was assumed here that this system is linear time invariant (LTI) and therefore we expect the main rotor blade pitch angle to change sinusoidally at the same frequency as the input sinusoidal signal. This assumption is tested in Section 6. This motion was recorded using a high-speed Sony video camera. The frequency of the sinusoidal input signal was increased repeatedly to obtain measurements over a number of frequencies. The amplitude of each measurement allows the gain from the collective to the main rotor blade pitch angle to be tabulated for each frequency considered, producing its amplitude plot. The final step in this system identification procedure was to fit a transfer function to the measured amplitude plot.

The image processing theory used is introduced in Section 2 and is applied in Section 3 where the image processing algorithm is explained. Results showing each stage of the algorithm are also given. Section 4 describes the system identification process employed. Practical issues regarding the experimental setup

are given in Section 5. The results of the system identification process are discussed in Section 6.

## 2. Image Processing Theory

The algorithm described in Section 3 performs image segmentation by thresholding. Image moments are used to calculate the orientation of the rotor blades by extracting the location of coloured stickers placed on the blade.

Image segmentation involves decomposing an image into regions, such as a foreground object and the background it appears against [4]. Thresholding is one simple technique that is widely used in image segmentation [5]. The resulting output image is known as a binary image when only two regions are detected. Segmentation through thresholding has been applied in the extraction of details from sequences of X-ray images [6], as well as the identification of buildings within images [7].

The location of an object can be determined in a number of ways, one of which is by finding the object's centre of mass, also known as its centroid [4]. The location of the centroid is found by calculating the area of the object of interest in pixels as well as the image's first moments along the x and y axes. The general two-dimensional Cartesian moment of order $(p + q)$ is $m_{pq}$ and is defined as [8]:

$$m_{pq} = \int_{-\infty}^{\infty} \int_{-\infty}^{\infty} x^p y^q I(x, y) \, dx dy \qquad (1)$$

The function $I(x, y)$ assigns a weight to each $(x, y)$ coordinate in the image and is analogous to a density function used in physics. The distance in pixels from the left-hand side of the image is $x$, while the distance in pixels from the top of the image is $y$. The order of the x-component of the calculation is given by $p$, while $q$ is the order of the y-component.

After discretization, and setting the area represented by each discrete point in the image equal to 1, the 1$^{st}$ order moments are defined as [8]

$$m_{10} = \sum_x \sum_y x I(x, y)$$
$$m_{01} = \sum_x \sum_y y I(x, y) \qquad (2)$$

The moment of order zero, or area of the image in pixels, is defined as

$$m_{00} = \sum_x \sum_y I(x, y) \qquad (3)$$

The coordinate of the centroid is defined relative to the image's coordinate system as

$$(\overline{x}, \overline{y}) = \left( \frac{m_{10}}{m_{00}}, \frac{m_{01}}{m_{00}} \right) \qquad (4)$$

The centroid was chosen due to the relative ease with which it may be found. It is less robust to poor segmentation, where only a part of the sticker is detected. However, as a large degree of control can be exercised over the environment and the disturbances in that environment, the image processing algorithm does not need to employ special techniques such as the circle Hough transform to determine the coordinates of the stickers.

Image moments have been used in various forms with applications in pattern recognition applications such as visual servoing in robotics [9].

A recent trend in image processing is to make use of the massively parallel architecture of Graphics Processing Units
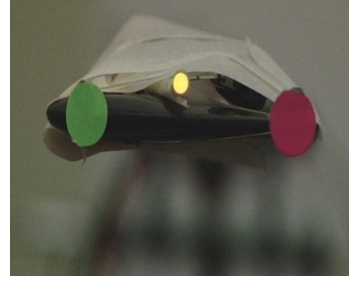


Figure 1: *The camera's view of the main rotor showing the two stickers that must be detected and a status LED. The LED is deactivated when a signal is applied to the collective control.*
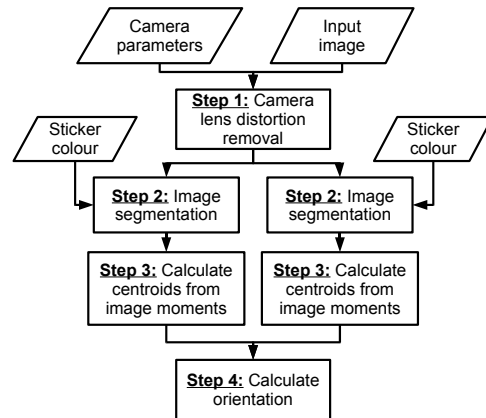


Figure 2: *Image processing algorithm stages.*

(GPU) to accelerate the processing of an image [10]. The reason for this shift is that most image processing involves performing the same operation on each pixel in an input image. The GPU of a computer is able to process multiple pixels in parallel, producing a substantial performance increase when compared to the Central Processing Unit (CPU) of a computer, making it attractive for use in this processing intensive field [10]. Applications that execute on GPUs are known as Shaders when used within a graphics system such as the XNA Framework that was used here.

## 3. Image Processing Algorithm

An algorithm was developed to determine the orientation of the rotor blade in question. Two coloured stickers were placed on the edge of the rotor blade as shown in Figure 1 to allow the leading and trailing edges of the rotor blade to be identified. This algorithm extracts each sticker and finds their centroids, after which the orientation of the line joining the centroids is found.

A four-step process is followed as shown in Figure 2. Segmentation is performed twice, once for each sticker, producing two segmented images containing the separate stickers. Each sticker has a different colour, allowing them to be detected individually. The centroid of each sticker is calculated using (4). The final step is to calculate the angle of the line joining the centroids of the two stickers.

Camera lens distortion was modelled using a 6$^{th}$ order model which accounts for radial and tangential distortion [11]. Tangential distortion is introduced when the principle point, or centre, of the camera's lens is not directly above the centre of the camera's
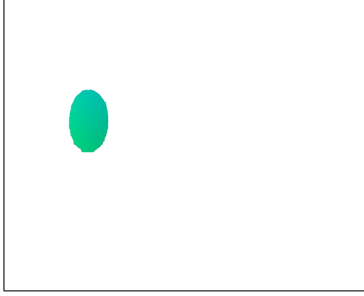
Figure 3: *The result of applying segmentation to the input image. The chosen threshold colour was that of the left hand sticker.*
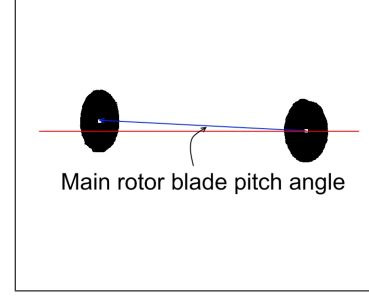


Figure 4: *The result of applying the image processing algorithm to an input image. The centres of each sticker, as determined by the algorithm, are shown.*

sensor. This problem is more apparent when working with a zoom lens.

During segmentation, each pixel that matches the sticker colours, is replaced with its location, as well as a flag to indicate that the pixel matched the sticker colour. As the implementation runs on a GPU as a Shader, the flag and position are stored in the colour components of the output pixels. The result of applying segmentation to remove the background from Figure 1 is shown in Figure 3.

Step 3 calculates the above moments for 2x2 blocks of pixels in the segmented images and encodes the results as pixels in a new image. The resulting image is half the width and height of the input image. The function $I(x, y)$ used in calculating the moments, is the flag value generated in step 2 for each pixel. This parallel reduction operation was implemented as a Shader on the GPU. This process is repeated until the resulting image no longer has dimensions which are even numbers. If the number of repetitions is $N$ then each pixel in the resulting image represents the average value of $4^N$ pixels from the original segmented image. At this point, the algorithm returns to the CPU where the final resultant image's pixels are averaged. The result of this process is the average colour of the segmented image.

This average colour contains the area of the sticker in pixels, as well as the $1^{st}$ moments in the x and y directions. However, since each sub-block of pixels was averaged, the resulting moments are all scaled by the number of pixels averaged at each stage on the GPU, i.e. $4^N$.

The line joining the centroids can now be found and is assumed to be from the second sticker to the first. The final result of applying this process to Figure 1 is shown in Figure 4. The location of the main rotor blade pitch angle is indicated for clarity. The centroids of both stickers have been correctly detected and are shown by the white squares in the binarized images of each sticker. The line joining the stickers has been indicated, as well as a horizontal reference line.

## 4. System Identification Theory

The objective of system identification is to determine a model of an unknown system using experimental methods [12]. Various approaches exist, depending on how much is known about the system. In the case of an LTI model of a single-input single-output (SISO) system, the transfer function is described by

$$G(s) = \frac{b_{n_b} s^{n_b} + \ldots + b_1 s + b_0}{a_{n_a} s^{n_a} + \ldots + a_1 s + 1} \qquad (5)$$

where $G(s)$ is the continuous time transfer function of the system in the Laplace domain. The numerator and denominator are polynomials of order $n_b$ and $n_a$ respectively.

Their coefficients are $b_i$ and $a_j$, where $i = 0, 1, \ldots, n_b$ and $j = 1, 2, \ldots, n_a$.

The system identification procedure entails determining the coefficients in the numerator and denominator from frequency domain measurements. From theory, it is known that an LTI system will produce a sinusoidal response to a sinusoidal input and that the response will have the same frequency as the input signal, but a different amplitude and phase [13].

This gives rise to the technique of frequency response analysis by means of sine wave testing [12]. Small amplitude input signals are used to ensure operation within the system's linear region. They must, however, be large enough to be meaningful in future applications. The system identification procedure proceeds as follows:

1. Apply a sinusoidal input with known frequency and amplitude to the collective control.
2. Measure the amplitude of the sinusoidal output (the main rotor blade pitch angle) using the image processing algorithm from Section 3.
3. Calculate the gain of the system at the test frequency. This gain is the ratio of the amplitude of the output signal to the amplitude of the input signal.
4. Repeat this process at a number of test frequencies to obtain an amplitude plot over the range of frequencies of interest.

The amplitude plot that is constructed forms a nonparametric model of the system [14], from which a parametric model, (5), must be derived. A nonlinear regression problem may be formulated by fitting the magnitude, $|G(s)|$ of the transfer function to the measured amplitude spectrum. Nonlinear regression is used as the magnitude function contains squares of the real and complex components of the transfer function and therefore, cannot be represented as a linear least squares regression problem. The MATLAB function `nlinfit` was used to solve this problem [15].

The order of the transfer function must be estimated graphically from the amplitude plot before performing the nonlinear regression analysis. A procedure that may be applied to analyse the asymptotic log-magnitude plot is given by Nagrath and Gopal [16].

The approach used here does not rely on the phase difference between the input and output signals as this difference cannot be measured accurately with the camera used in this experiment as the frame rate of the camera is insufficient. The camera cannot be synchronized to the control input signal either. An expensive solution is to use a camera which supports the Camera Link® interface standard [17]. These cameras include a trigger input,
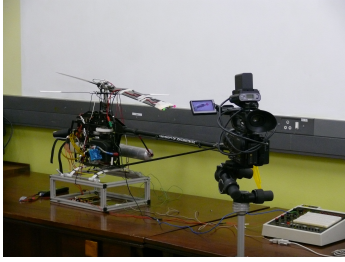
Figure 5: *The measurement setup, showing the high-speed Sony camera and helicopter.*



Figure 6: *Maximum theoretical error for measurement of angles in the range $0°$ to $20°$ as a function of the distance between sticker centroids.*



Figure 7: *The measured main rotor blade pitch angle and fitted cosine function as a function of time for a single frequency.*

which controls the time at which frames are captured and allows the capture of frames to be synchronized with the control input signal.

The approach used here is justified as a pole or zero has the same effect on the amplitude plot of a system, irrespective of the sign of its real component [18]. Therefore, only the sign of the real component cannot be determined from the amplitude plot. Since the system being characterized is known to be stable, the assumption can be made that all real components of the poles and zeros are negative, as this is a requirement for a stable linear system [13]. If it were not so, the main rotor would violently tear itself loose at the slightest control input.

## 5. Experimental Setup

A high-speed camera is placed such that it faces the edge of one of the main rotor blades. Two stickers, of different colours, are affixed to the rotor blades, as seen in Figure 1. The camera should be placed as close as possible to the rotor blade, or a powerful zoom lens must be used, to allow maximum utilization of the available image space. A Sony HD video camera, HVR-Z7E, was used as it supports high-speed video at 100 frames per second. The arrangement used is shown in Figure 5.

A yellow LED was attached to the edge of the rotor blade for use as a signal to indicate when the collective control input was applied. This allows the time delay between applying a control action and detecting a response, to be estimated. This time delay is known as the system's dead time [19] and must be taken into account when designing future control systems.

This experiment was performed under static conditions. The engine was not active and hence the rotor blades were not rotating at the time. No additional weights were attached to the rotor blades to simulate the load that the servo motors would encounter during flight.

An error analysis was performed to quantify what image resolution was needed to obtain a certain upper limit on the quantization noise introduced by the image processing method. The assumption made in this analysis was that the quantization error in the measurement of the centre of the stickers would be at most 1 pixel in error in either the x or y, or both directions. As the implementation makes use of 32-bit floating-point numbers throughout the calculations, which are accurate to approximately 7 digits, the position of the sticker's centroids can be calculated with subpixel accuracy. Therefore, the assumption of a 1 pixel quantization error is overly pessimistic. This analysis does not consider the error introduced by partial detection of a sticker since that is not influenced by camera resolution.

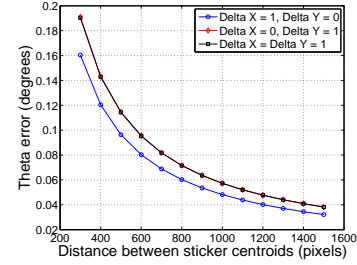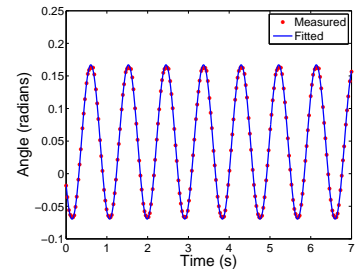The results of this analysis are shown in Figure 6. As the Sony camera provides a resolution of 720x576 pixels, it is likely that the stickers will be approximately 600 pixels apart if the rotor blade fills the camera's view. Therefore, the quantization error will be at most $0.1°$ or $0.0017\,\mathrm{rad}$.

Additional errors are introduced if the two stickers are not placed exactly on the chord of the rotor blade. The measurements of the orientation will contain a constant error as the line joining the stickers will probably not be parallel to the blade's chord. This does not present a problem for the system identification as the amplitude of the sinusoidal oscillation is used, instead of the peak values.

## 6. Results and Analysis

The system identification process described in Section 4 was applied. An example of the measured main rotor blade pitch angle as a function of time for one of the test frequencies is shown in Figure 7. The amplitude and frequency of these sinusoids were determined by fitting a cosine function to the measurements, as indicated in Figure 7. This allowed all of the frames that were captured to be taken into account, reducing the error in the measurement due to sampling and other unknown noise sources. This approach also allows the quality of the sinusoidal outputs to be measured and is known as sinusoidal fidelity [20]. This technique can expose nonlinear systems.

From Figure 7, it is apparent that the fitted sinusoid is an accurate estimate of the measured data. This is further confirmed by the plot of the error between the fitted sinusoid and the actual measurements given in Figure 8, which shows that the peak error is significantly smaller than the amplitude of the sinusoid. Figure 8 shows that the error is periodic and that the maximum error occurs at the peaks and troughs of the fitted sinusoid. This was observed at all frequencies. At these points, the system demonstrates nonlinear behaviour as the measured values flatten out, rather than continuing to follow a sinusoid. This may be due
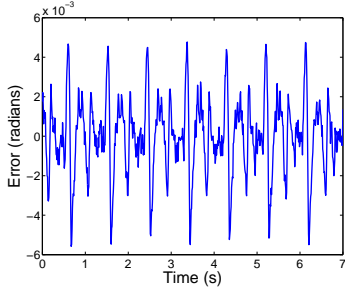
Figure 8: *The error in radians between the fitted sinusoid and the measured data.*
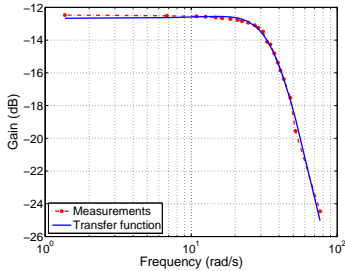


Figure 9: *Amplitude plot of the measured transfer function and the fitted transfer function.*



Figure 10: *The estimated and measured step responses.*



Figure 11: *The improved step response estimation after setting $\zeta = 0.8$.*

to quantization of the input signal to the servo motors. Saturation in the system is not the cause as the step response shown later indicates that the system is capable of producing a much larger angle than tested during the frequency sweep.

Throughout the characterization experiment, an offset of approximately $0.05\,\mathrm{rad}$ or $2.8°$ was observed. This appears to be due to incorrect placement of the stickers.

Figure 9 shows the amplitude data which was measured during the experiment. It is apparent that the $-3\,\mathrm{dB}$ bandwidth of the system is approximately $40\,\mathrm{rad\,s^{-1}}$ or $6\,\mathrm{Hz}$. Using graphical means, the slope of the log-magnitude plot at high frequencies was found to be approximately $-40\,\mathrm{dB}$ per decade, suggesting that the system is a $2^{\mathrm{nd}}$ order system. After performing an initial system identification, a second-order transfer function was found to fit the measured data. This function is shown in Figure 9. This transfer function was

$$G\left(s\right) = 0.23 \frac{\left(37^2\right)}{s^2 + 2\left(0.65\right)\left(37\right)s + 37^2} \qquad (6)$$

The gain of this system is approximately $0.23\,\mathrm{rad}$, or $13°$, while it's natural frequency $\omega_n$ and damping ratio $\zeta$ were found to be $37\,\mathrm{rad\,s^{-1}}$ and $0.65$ respectively. Mettler identified a similar natural frequency of $39.18\,\mathrm{rad\,s^{-1}}$, but found the damping ratio to be $1.22$, corresponding to an overdamped system [2]. This may be attributed to the use of different servo motors as they may provide a greater internal damping force. The gain cannot be compared as Mettler measures swashplate deflection rather than blade pitch. The $2^{\mathrm{nd}}$ order approximation used by Gavrilets used $\omega_n = 44\,\mathrm{rad\,s^{-1}}$ and $\zeta = 0.6$ [1], while the gain was reported as $0.183\,\mathrm{rad}$, which demonstrates that the results obtained here are reasonable.

The results of this system identification were tested by measuring the step response and comparing that to the predicted step response of the identified transfer function as shown in Figure 10.
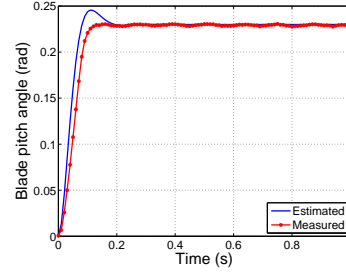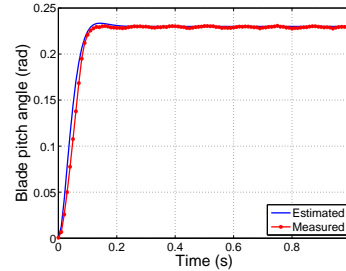
The predicted step response demonstrates overshoot of approximately $0.02\,\mathrm{rad}$ or $9\,\%$ as expected from the damping ratio. However, this overshoot was not observed in the measurements. The system's gain and the settling time of approximately $0.2\,\mathrm{s}$ have been captured accurately. The oscillation that is present in the measurements after approximately $0.2\,\mathrm{s}$ appears to be related to the natural frequency of the rotor blade structure, as vertical vibrations, or flapping, were observed while characterizing the system at frequencies between approximately $8\,\mathrm{Hz}$ and $10\,\mathrm{Hz}$, indicating resonance at these frequencies. The oscillation disappears after approximately $5\,\mathrm{s}$. The measured $10\,\%$ to $90\,\%$ rise time of approximately $70\,\mathrm{ms}$ is comparable to Pettersen [3].

A second iteration showed that a damping ratio of $0.8$ produced a more accurate approximation as shown in Figure 11. The new estimated transfer function is shown in Figure 12, where it is apparent that the frequency response is not correctly estimated. Repetition of the characterization yielded the same transfer function as (6). Research suggests that the digital control system present in the servo motors may be the cause of this nonlinear behaviour. The original estimate of $\zeta = 0.65$ was retained to ensure acceptable accuracy over the frequency range that was tested.

The time delay present in the system was measured by observing how many frames were captured between switching off the LED mentioned earlier, and the rotor blade beginning to move. This delay was found to be approximately $85\,\mathrm{ms} \pm 5\,\mathrm{ms}$. This is reasonable as a delay of $20\,\mathrm{ms}$ is introduced, as a servo motor's input signal is a $50\,\mathrm{Hz}$ pulse width modulated signal. As anticipated, the servo controller software and the RS232 connection to the controlling computer introduced additional delays exceeding $20\,\mathrm{ms}$.

## 7. Conclusion

A method has been demonstrated for the identification of a transfer function for a linear time invariant single-input single-
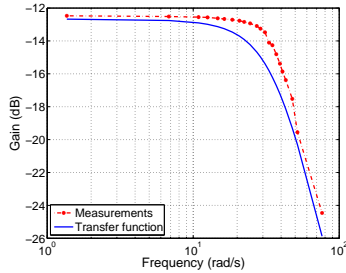
Figure 12: *The amplitude plot of the transfer function model with $\zeta = 0.8$.*

output system using a high-speed camera and performing image processing. The system in question was the servo motors and mechanical connections linking the collective control input of a model helicopter to the main rotor blades. An image processing algorithm that measures the orientation of a rotor blade using segmentation and image moments, was explained. This algorithm detects two coloured stickers placed on the rotor blades. This algorithm is generic enough to be applied to other systems where the measured output is the orientation of an object. Potential sources of errors were discussed and methods of eliminating or reducing them were covered.

The main rotor blade pitch angle was measured while driving the collective control input with a sinusoidal signal. The frequency of this sinusoid was varied to obtain an amplitude plot of the system's transfer function. Nonlinear regression was used to fit this amplitude plot to a $2^{nd}$ order transfer function. The bandwidth of this system, from the collective control input to the main rotor blade pitch angle, was found to be approximately $6\,\mathrm{Hz}$, while system dead time was measured as $85\,\mathrm{ms}$. Therefore, this result is significant for future control system development as it is likely that such a control system will be sampled at a higher frequency than this bandwidth.

Comparison of the estimated and actual step responses in this experiment showed some differences, which appear to be as a result of nonlinear elements within the system. The original transfer function estimate was accepted as it appears to provide good overall accuracy over the range of frequencies tested. This transfer function has $\omega_n = 37\,\mathrm{rad\,s^{-1}}$ and $\zeta = 0.65$, while its gain is $0.23\,\mathrm{rad}$. These results are similar to the literature [1] [2] [3]. Based on these results, the author believes that the assumption of linear time invariance is acceptable.

As this work was conducted under static conditions, it cannot be considered to be an accurate measurement of the response encountered during actual flight conditions. This experiment has demonstrated that this image processing based technique can be applied successfully, opening the way for possible future work in which dynamic conditions are considered.

# 8. References

[1] V. Gavrilets, ''Autonomous aerobatic manoeuvring of miniature helicopters,'' Ph.D. dissertation, Massachusetts Institute of Technology, May 2003.

[2] B. Mettler, *Identification Modelling and Characteristics of Miniature Rotorcraft*. Boston, Massachusetts: Kluwer Academic Publishers, 2003.

[3] R. Pettersen, E. Mustafic, and M. Fogh, ''Nonlinear Control Approach to Helicopter Autonomy,'' Master's thesis, Aalborg University, 2005.

[4] J. C. Russ, *The Image Processing Handbook*, 4th ed. New York: CRC Press, 2002.

[5] G. X. Ritter and J. N. Wilson, *Handbook of Computer Vision Algorithms In Image Algebra*, 2nd ed. CRC Press, 2001.

[6] Y. Bentoutou and N. Taleb, ''Automatic Extraction of Control Points for Digital Subtraction Angiography Image Enhancement,'' *IEEE Transactions on Nuclear Science*, vol. 52, no. 1, Feb. 2005.

[7] J. F. Gilmore and W. W. Boyd, ''Building and Bridge Classification by Invariant Moments,'' in *SPIE*, Aug. 1981.

[8] M. Nixon and A. Aguado, *Feature Extraction & Image Processing*. Newnes, 2004.

[9] O. Tahri and F. Chaumette, ''Point-Based and Region-Based Image Moments for Visual Servoing of Planar Objects,'' *IEEE Transactions on Robotics*, vol. 21, no. 6, pp. 1116--1127, Dec. 2005.

[10] Y. Roodt, W. Visser, and W. A. Clarke, ''Image Processing on the GPU: Implementing the Canny Edge Detection Algorithm,'' in *PRASA*, 2007.

[11] Camera Calibration Toolbox for Matlab. California Institute of Technology. [Online]. Available: http://www.vision.caltech.edu/bouguetj/calib_doc/htmls/parameters.html

[12] L. Ljung, *System Identification: Theory for the User*, ser. Prentice-Hall Information and System Sciences Series. Englewood Cliffs, New Jersey: Prentice-Hall, 1987.

[13] R. E. Ziemer, W. H. Trantler, and D. R. Fannin, *Signals & Systems: Continuous and Discrete*, 4th ed. New Jersey: Prentice Hall, 1998.

[14] M. B. Tischler and R. K. Remple, *Aircraft and Rotorcraft System Identification: Engineering Methods with Flight--Test Examples*, ser. AIAA Education Series. Reston, VA: American Institute of Aeronautics and Astronautics, Inc., 2006.

[15] The MathWorks. (2009, Sep.) nlinfit. [Online]. Available: http://www.mathworks.com/access/helpdesk/help/toolbox/stats/index.html?/access/helpdesk/help/toolbox/stats/nlinfit.html

[16] I. J. Nagrath and M. Gopal, *Control Systems Engineering*. New Delhi: Wiley Eastern Limited, 1978.

[17] T. A. I. Association. (2000, Oct.) Camera Link: Specifications of the Camera Link Interface Standard for Digital Cameras and Frame Grabbers. Version 1.0. [Online]. Available: http://www.vision1.com/pdf/CameraLink5.pdf

[18] J. J. D'Azzo and C. H. Houpis, *Linear Control System Analysis and Design Conventional and Modern*, 2nd ed., ser. McGraw-Hill series in electrical engineering. Tokyo: McGraw-Hill, 1983.

[19] C. Brosilow and B. Joseph, *Techniques of Model-based Control*, ser. Prentice Hall International Series in the Physical and Chemical Engineering Sciences, N. R. Amundson, Ed. Upper Saddle River, NJ: Prentice Hall PTR, 2002.

[20] S. W. Smith, *The Scientist and Engineer's Guide to Digital Signal Processing*. California Technical Pub., 1997.